BRAIN
ORIGINAL ARTICLE

Early stages of tau pathology and its associations with functional connectivity, atrophy and memory

David Berron,[1] Jacob W. Vogel,[2] Philip S. Insel,[1,3] Joana B. Pereira,[4] Long Xie,[5,6] Laura E. M. Wisse,[5,6,7] Paul A. Yushkevich,[5,6] Sebastian Palmqvist,[1,8] Niklas Mattsson-Carlgren,[1,9,10] Erik Stomrud,[1,8] Ruben Smith,[1,9] Olof Strandberg[1] and Oskar Hansson[1,2]

In Alzheimer's disease, post-mortem studies have shown that the first cortical site where neurofibrillary tangles appear is the transentorhinal region, a subregion within the medial temporal lobe that largely overlaps with Brodmann area 35, and the entorhinal cortex. Here we used tau-PET imaging to investigate the sequence of tau pathology progression within the human medial temporal lobe and across regions in the posterior-medial system. Our objective was to study how medial temporal tau is related to functional connectivity, regional atrophy, and memory performance.

We included 215 amyloid-β– cognitively unimpaired, 81 amyloid-β+ cognitively unimpaired and 87 amyloid-β+ individuals with mild cognitive impairment, who each underwent ^{18}F-RO948 tau and ^{18}F-flutemetamol amyloid PET imaging, structural T_1-MRI and memory assessments as part of the Swedish BioFINDER-2 study. First, event-based modelling revealed that the entorhinal cortex and Brodmann area 35 show the earliest signs of tau accumulation followed by the anterior and posterior hippocampus, Brodmann area 36 and the parahippocampal cortex. In later stages, tau accumulation became abnormal in neocortical temporal and finally parietal brain regions. Second, in cognitively unimpaired individuals, increased tau load was related to local atrophy in the entorhinal cortex, Brodmann area 35 and the anterior hippocampus and tau load in several anterior medial temporal lobe subregions was associated with distant atrophy of the posterior hippocampus. Tau load, but not atrophy, in these regions was associated with lower memory performance. Further, tau-related reductions in functional connectivity in critical networks between the medial temporal lobe and regions in the posterior-medial system were associated with this early memory impairment. Finally, in patients with mild cognitive impairment, the association of tau load in the hippocampus with memory performance was partially mediated by posterior hippocampal atrophy.

In summary, our findings highlight the progression of tau pathology across medial temporal lobe subregions and its disease stage-specific association with memory performance. While tau pathology might affect memory performance in cognitively unimpaired individuals via reduced functional connectivity in critical medial temporal lobe-cortical networks, memory impairment in mild cognitively impaired patients is associated with posterior hippocampal atrophy.

1 Clinical Memory Research Unit, Department of Clinical Sciences Malmö, Lund University, 223 62 Lund, Sweden
2 Department of Psychiatry, University of Pennsylvania, Philadelphia, PA 19104, USA
3 Department of Psychiatry and Behavioral Sciences, University of California, San Francisco, CA 94143, USA
4 Division of Clinical Geriatrics, Department of Neurobiology, Care Sciences and Society, Karolinska Institute, 171 77 Stockholm, Sweden
5 Penn Image Computing and Science Laboratory (PICSL), University of Pennsylvania, Philadelphia, PA 19104, USA

6   Department of Radiology, University of Pennsylvania, Philadelphia, PA 19104, USA
7   Department of Diagnostic Radiology, Lund University, 221 00 Lund, Sweden
8   Memory Clinic, Skåne University Hospital, 205 02 Malmö, Sweden
9   Department of Neurology, Skåne University Hospital, 221 00 Lund, Sweden
10 Wallenberg Center for Molecular Medicine, Lund University, 221 00 Lund, Sweden

Correspondence to: David Berron
Clinical Memory Research Unit
Department of Clinical Sciences Malmö, Lund University
Sölvegatan 19, 223 62 Lund, Sweden
E-mail: david.berron@dzne.de

Correspondence may also be addressed to: Oskar Hansson
E-mail: oskar.hansson@med.lu.se

Introduction

Tau pathology is closely associated with cognition[1] and particularly with memory performance in Alzheimer's disease.[2] Studies on the functional architecture of memory have identified two major cortical memory networks that are highly connected with the hippocampus and differentially involved in episodic memory—the anterior-temporal and the posterior-medial system.[3,4] While early amyloid-β deposition occurs in regions of the posterior-medial system such as the posterior cingulate cortex and the precuneus,[5–7] neurofibrillary tangle accumulation occurs early in medial temporal lobe (MTL) subregions of the anterior-temporal system.[2,8,9]

Specifically, neurofibrillary tangles have been described to appear first in the transentorhinal region, a subregion within the MTL that largely overlaps with Brodmann area 35, as well as in the entorhinal cortex.[8] Later, neurofibrillary tangles can be found in hippocampal subfield cornu ammonis (CA) 1 before they extend to adjacent regions such as the subiculum and then brain regions outside the MTL.[8,10]

While tau begins to accumulate in MTL regions in the anterior-temporal system, it can be increasingly seen in regions in the posterior-medial system with disease progression.[11,12] Furthermore, tau pathology is tightly linked to atrophy and future neurodegeneration, and both are associated with cognitive impairment,[13–15] which likely affects cognitive functions associated with the anterior-temporal system before those associated with the posterior-medial system.

In order to understand to what extent functional memory networks are affected during the course of Alzheimer's disease, it is important to know the exact order of tau pathology progression throughout subregions in the MTL and the cortical posterior-medial system. However, to date this remains unknown as neuropathological studies have not studied tau pathology across all these subregions in the same individuals. It is also unclear whether tau pathology leads to cognitive impairment primarily via grey matter atrophy, or whether there are changes in other modalities, such as functional connectivity that may precede gross atrophy, especially in early stages of Alzheimer's disease.[16]

With the recent advent of tau-PET, it has become possible to investigate the accumulation of tau pathology *in vivo*, and second generation tau-PET tracers now allow the investigation of hippocampal tau-PET binding due to reduced off-target binding in the choroid plexus.[17] Here, we use ^{18}F-RO948 tau-PET imaging in combination with event-based modelling (EBM)[18] to characterize the sequence of tau-PET binding in MTL subregions, including MTL regions of the anterior-temporal system, and the cortical posterior-medial system in cognitively unimpaired individuals and patients with mild cognitive impairment (MCI). We utilize whole brain analyses as well as MTL subregional segmentation[19] to investigate how tau-PET binding is associated with functional connectivity, memory function and atrophy.

Materials and methods

Participants

We analysed data from 383 non-demented individuals from the Swedish BioFINDER-2 study (NCT03174938), which was approved by the ethical review board in Lund, Sweden. Participants were enrolled between 2017 and 2020 and gave their written informed consent to participate. Participants were stratified into cognitively unimpaired individuals and patients with MCI (see Supplementary material for details on inclusion criteria and missing data). Amyloid-β status (positive/negative) was defined using CSF amyloid-$β_{42/40}$ (cut-off 0.63).

Twenty-five individuals were excluded during quality assessment of automated MTL subregional segmentations [nine cognitively unimpaired (CU) amyloid-β–, six CU amyloid-β + and 10 MCI amyloid-β +]. As ^{18}F-RO948 tau PET shows off-target binding in the skull and the meninges in some individuals that could interfere with tau-PET signal in MTL subregions, we calculated a ratio of tau-PET signal in the skull/meninges compared to signal in grey matter to identify individuals with high amounts of off-target binding [> 1.5 standard deviation (SD), $n = 37$]. Subsequently, each case was visually assessed and excluded in case of confirmed bleeding of off-target binding signal from the meninges in MTL subregions ($n = 17$).

Imaging acquisition

MRI

T_1-weighted images were acquired on a Siemens Prisma scanner (Siemens Medical Solutions) with a 64-channel head coil using an MPRAGE sequence (in-plane resolution = 1×1 mm^2, slice

thickness = 1 mm, repetition time = 1900 ms, echo time = 2.54 ms, flip-angle = 9°). Spontaneous blood oxygen level-dependent (BOLD) oscillations were acquired with a gradient-echo planar sequence (eyes closed, in-plane resolution = 3×3 mm^2, slice thickness = 3.6 mm, repetition time = 1020 ms, echo time = 30 ms, flip-angle = 63°, 462 dynamic scans, 7.85 min).

Tau and amyloid-β PET

All study participants underwent PET scans on a digital GE Discovery MI scanner (General Electric Medical Systems). Approval for PET imaging was obtained from the Swedish Medical Products Agency. Participants were injected with 365 ± 20 MBq of ^{18}F-RO948, and LIST mode emission data were acquired for each scan 70–90 min (^{18}F-RO948) post-injection. Amyloid-β PET imaging was performed on the same platform 90–110 min after the injection of ~185 MBq ^{18}F-flutemetamol.[20]

Imaging analysis

Region of interest segmentation and estimates of volume and thickness

Individual volume and median thickness of MTL subregions including anterior (3416 mm^3, SD = 291) and posterior hippocampus (3206 mm^3, SD = 470), perirhinal cortex [divided in Brodmann area 35 (1202 mm^3, SD = 204) and Brodmann area 36 (3754 mm^3, SD = 604)], entorhinal (1094 mm^3, SD = 171) and parahippocampal cortex (1952 mm^3, SD = 582) were defined on T_1-weighted images ($1 \times 1 \times 1$ mm^3 resolution) using ASHS-T1[19] (Supplementary material) and a multi-template thickness analysis pipeline.[21] All subregional masks were visually assessed. Regions of interest for non-MTL regions such as inferior temporal (20 337 mm^3, SD = 2880), middle temporal (20 512 mm^3, SD = 2842), retrosplenial [isthmus cingulate (5078 mm^3, SD = 746), inferior parietal (24 518 mm^3, SD = 3575), posterior cingulate cortex (6029 mm^3, SD = 869) and precuneus (19 121 mm^3, SD = 2426)] were derived from T_1-weighted scans using FreeSurfer v6.0 (https://surfer.nmr.mgh.harvard.edu/).

Standardized uptake value ratio measures

^{18}F-RO948

Standardized uptake value ratio (SUVR) images were calculated for each subregion of interest using an inferior cerebellar reference region.[22] Partial volume correction was performed using the geometric transfer matrix method[23] extended to voxel-level using region-based voxel-wise correction.[24] To reduce the influence of off-target binding, choroid plexus tau-PET signal was regressed from hippocampal measures.

^{18}F-flutemetamol

A cortical composite SUVR was calculated using the whole cerebellum as reference region.[25]

Event-based modelling

An EBM framework was used to derive a sequence of brain regions that become sequentially abnormal based on their individual tau-PET SUVR.[18] The biomarkers in our analysis constitute 11 transition 'events' (tau-PET SUVR in Brodmann areas 35 and 36, entorhinal and parahippocampal cortex, anterior and posterior hippocampus, inferior and middle temporal cortex, inferior parietal and retrosplenial cortex and precuneus), where each event corresponds to a biomarker becoming abnormal with high probability. The most likely ordering of events and the respective uncertainty was estimated using the EBM,[18,26] where each biomarker

is either treated as 'normal', i.e. non-pathological, or 'abnormal'. Individual regional tau-PET SUVR from regions of interest were z-standardized and probabilistic cut-offs were derived using Gaussian mixture modelling as previously described.[27] Specifically, for each region of interest, we fit a two-component mixture model to the SUVR vector and used repeated 5-fold cross-validation to determine the probability a given value falls within the right-most (i.e. abnormal) Gaussian distribution. This resulted in a probability value between 0 and 1 that an individual regional SUVR was abnormal. We repeated this process to find the probability each SUVR was normal, and these two subject × region probability matrices were used as input to the EBM algorithm. Code for the probability estimation can be found at: https://github.com/illdo pejake/data_driven_pathology/blob/master/esm/ESM_utils.py; accessed 13 August 2021. EBM was run using the MATLAB implementation of EBM-SuStaIn with $k = 1$ (https://github.com/ucl-pond; accessed 13 August 2021). In this implementation, an 'event' represents the switch from a normal to an abnormal state. The EBM calculates the event sequence that maximizes the data likelihood, which in turn represents the most likely ordering of the events. In addition to defining the most likely event sequence, the EBM evaluates the relative likelihood of the position of each event along the sequences using Markov chain Monte Carlo resampling. This provides information about the uncertainty of the event ordering. In addition, the EBM provides an individual stage (0–11, corresponding to the number of biomarkers) for each participant, indicating which stage of the sequence of abnormal tau events that participant has reached. More details on the EBM and the calculation of uncertainties can be found in Young et al.[18] For visualization, tau-PET SUVR from individual regions of interest was regressed against tau-PET stages derived from the EBM using monotone non-linear splines where the Akaike information criterion was used to select the number of knots. Uncertainties represent 95% confidence intervals from the model estimated variance-covariance matrix.

Voxel-wise tau-PET analyses

Non-smoothed and partial volume corrected tau-PET SUVR images were transformed to template space using the non-linear warp obtained by normalizing the T_1-weighted image to the MNI152 template.[28] SUVR images from individuals were binned into four different groups across EBM stages with increasing disease severity with the aim to result in groups of roughly comparable size [stage 0 ($n = 281$), stage 1–3 ($n = 35$), stage 4–8 ($n = 29$), stage 9–11 ($n = 38$)] (Supplementary Table 6). For voxel-wise group comparisons of SUVR images, we used the Statistical Parametric Mapping software (SPM, Version 12; Wellcome Trust Centre for Neuroimaging, London, UK). Two-sample t-tests were used to contrast tau-PET SUVR images from groups of individuals in higher stages against those in stage 0 with the aim to visualize tau-PET signal binding for the different stages. Voxel-wise results were corrected using family-wise error (FWE) correction at a threshold of $P < 0.05$ and a cluster size of 50 mm^3.

Voxel-based morphometry

T_1-weighted images were preprocessed using SPM12. All images were segmented into grey matter, white matter, and CSF. Then, the diffeomorphic non-linear image registration tool (DARTEL)[29] was used to create a study-specific template based on the grey and white matter tissues of the whole sample. Once the template was created, the grey matter tissues were warped into MNI space using the individual flow fields resulting from the DARTEL registration, and voxel values were modulated for volumetric changes introduced by the normalization. Finally, the images were smoothed with an isotropic Gaussian kernel with 4 mm full-width at half-

maximum. To account for differences in head size in the statistical analyses in addition to age and sex, we calculated the total intracranial volumes of each subject as the sum of the grey matter, white matter and CSF volumes. All results were adjusted for multiple comparisons using a family wise error rate correction set at $P < 0.05$ and a cluster size of 50 mm³.

Resting state functional MRI preprocessing

Resting state functional MRI (rs-fMRI) data preprocessing was performed with a pipeline composed of FSL,[30] AFNI [31] and ANTS.[28] Anatomical processing involved skull stripping, segmentation of CSF, white and grey matter, and normalization to MNI152 space.[32] After bulk motion and slice timing correction, nuisance regression compensated white matter/CSF signal, physiological noise,[33] motion parameters [34] and scanner drift. Distortion correction was performed by unwarping the EPI average to a high resolution (1 × 1 × 1 mm³) T₂ scan.[35] Finally, the functional data were band-pass filtered (0.01–0.1 Hz) and transformed to MNI space. Frames causing outliers in total frame-to-frame signal variation (75 percentile plus 1.5 times interquartile range, IQR) were censored.[36] Subjects with a mean/maximum frame-wise displacement exceeding 0.7/3.0 mm were excluded.

The regions of interest in the template space atlas used in the connectivity analysis consisted of the BrainNetTome atlas,[37] in which the MTL subcortical regions were replaced with 50% thresholded probability fields generated by averaging all individual MTL subregional segmentations warped to template space. Regions of interest in the anterior-temporal/posterior-medial system were selected based on regions that showed significant functional connectivity with the MTL in amyloid-β cognitively unimpaired older adults as identified in a previous publication and subdivided in individual BrainNetTome regions.[16] In the functional connectivity analysis, network components involving connections between MTL subregions and anterior-temporal/posterior-medial subsystems[16] that correlated with regional tau-PET SUVR were extracted and corrected for age, sex and a cortical composite measure of amyloid-β PET. In a second stage of this calculation, subcomponents of the tau-correlating network component associated with memory performance were identified (Supplementary material).

Cognitive measure

As a measure representing episodic memory, we used the delayed 10-word list-recall test from the Alzheimer's Disease Assessment Scale-Cognitive Subscale (ADAS-Cog), measured on a scale from 0 to 10, with 0 being least impaired.[38] The learning trial of the 10 words was repeated three times. After a distraction task (Boston Naming Test: 15 items short version), the participant was asked to freely recall the 10 words ('delayed recall'). Delayed recall was scored as number of errors (i.e. 10 minus correct recalled words), so that a higher score equalled worse memory performance.

Statistical analysis

Multiple regression analyses were carried out between measures of tau and amyloid-β PET, MTL subregional atrophy and memory in Rv3.3.2 (www.r-project.org). All models were adjusted for sex, age and amyloid-β PET in addition to years of education (for models including cognitive measures) and intracranial volume (for models including volumes). Results were corrected for multiple comparisons using false discovery rate (FDR) correction ($P < 0.05$) where appropriate. Mediation models were calculated using the lavaan package using a bootstrap method for the mediation effect.[39] Robust regression models estimated using iteratively reweighted least squares (ILRS) were calculated using the MASS package (rlm function).

Data availability

Anonymized data will be shared by request from a qualified academic investigator for the sole purpose of replicating procedures and results presented in the article and as long as data transfer is in agreement with EU legislation on the general data protection regulation and decisions by the Ethical Review Board of Sweden and Region Skåne, which should be regulated in a material transfer agreement.

Results

Participant sample

The sample consisted of 217 amyloid-β– (CU amyloid-β–, 57% female, mean age 67 years) and 79 amyloid-β+ cognitively unimpaired older adults (CU amyloid-β+, 51% female, mean age 71) as well as 87 amyloid-β+ patients with MCI (56% female, mean age 72) (Table 1).

Accumulation of Alzheimer's disease pathology in MTL subregions and regions in the posterior-medial system

We used an EBM approach to derive a sequence of brain regions becoming abnormal with respect to accumulation of Alzheimer's disease pathology. Every region becoming abnormal represents an individual event in the EBM.[18] We were interested in the sequence of individual brain regions becoming abnormal with respect to tau accumulation in MTL subregions and across regions of the posterior-medial system. We found that tau-PET signal in the entorhinal cortex and Brodmann area 35 showed abnormality first and were followed by the anterior and posterior hippocampus, Brodmann area 36, parahippocampal, middle-temporal, inferior-temporal, inferior-parietal and retrosplenial cortex, and finally the precuneus (Fig. 1A). Individuals with positive amyloid status and cognitive impairment were assigned higher tau-EBM stages (Fig. 1B). Notably, cognitively unimpaired individuals were almost exclusively positioned in stages 0–6 where tau abnormality was limited to MTL subregions. Many amyloid-β+ MCI patients nonetheless presented with low tau-EBM stages. Supplementary Tables 7 and 8 compare sample characteristics and co-morbidities to amyloid-β+ MCI patients at high tau-EBM stages.

To visualize tau accumulation across tau-EBM stages, we regressed subregional tau-PET SUVR against tau-EBM stages for each individual and region of interest using non-linear splines (Fig. 1C). Entorhinal cortex and Brodmann area 35 showed the steepest increase before they reach a plateau around stage 8 and 10, respectively. Anterior and posterior hippocampus followed with less steep increases reaching a plateau around stage 6 and never reached similar levels compared to extrahippocampal regions. Brodmann area 36 and the parahippocampal cortex began to increase in stages 2–3, followed by middle-temporal, inferior-temporal and inferior parietal cortex, which started to increase in stages 4–5. Finally, retrosplenial cortex and precuneus began to increase in stage 7.

Stages 5–8 were less populated than other stages, which could theoretically have an influence on the observed dynamics in tau-PET increase across stages. Thus, we ran two additional analyses with less events, which yielded almost identical results (Supplementary Fig. 1).

Table 1 Participant characteristics

	CU amyloid-β– (n = 217)	CU amyloid-β + (n = 79)	MCI amyloid-β + (n = 87)	Total (n = 383)
Age, years	66.9 (10.1)	71.2 (8.54)	72.4 (6.89)	69.0 (9.48)
Education, years	12.6 (3.47)	12.7 (3.75)	13.3 (4.82)	12.8 (3.87)
Sex, female	57.1%	50.6%	56.3%	55.6%
MMSE[a]	29 (1.23)	28.9 (1.24)	26.7 (1.91)	28.4 (1.69)
Delayed-Word-Recall (errors)[b]	2.34 (1.64)	3.18 (1.51)	7.05 (2.31)	3.58 (2.62)

Mean values (SD) unless otherwise stated. Amyloid-β positivity was defined based on CSF amyloid-$\beta_{42/40}$ levels. CU = cognitively unimpaired; MMSE = Mini-Mental State Examination.
[a]MMSE is presented in points.
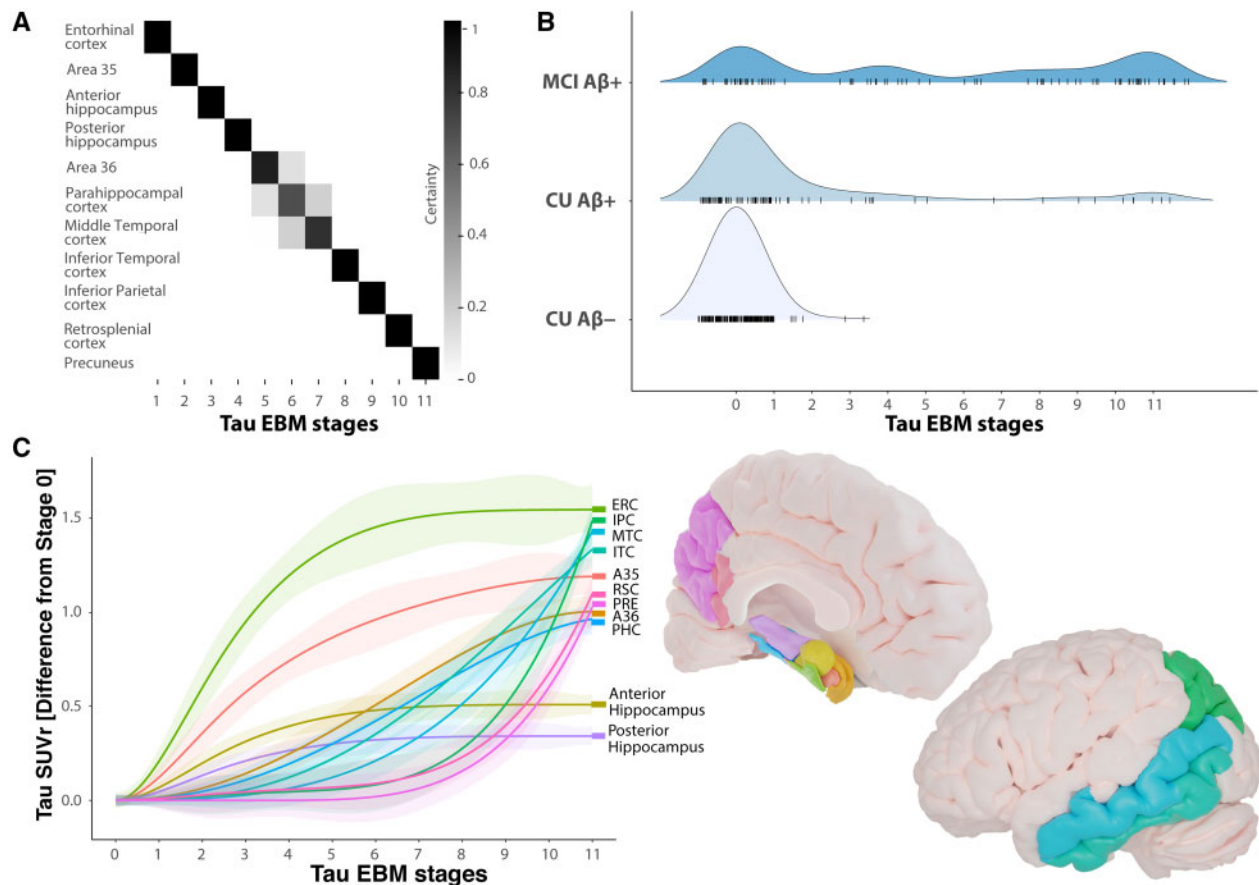[b]ADAS Delayed Word Recall is presented in number of errors.

Figure 1 Sequence of biomarker abnormality in non-demented older adults. (**A**) Positional variance plot for the EBM including tau-PET regions of interest in the MTL and posterior-medial system showing the distribution of event sequences. The positional variance diagram shows the uncertainty in the maximum likelihood event ordering estimated by taking MCMC (Markov chain Monte Carlo) samples using the EBM and each entry represents the proportion of MCMC samples in which events appear at a particular position in the sequence (x-axis). The proportion ranges from 0 in white to 1 in black. (**B**) Distributions of study participants in diagnostic groups across tau-EBM stages. (**C**) Non-linear splines visualizing differences in tau-PET SUVR across tau-EBM stages for individual regions of interest. Mean tau-PET SUVR from individuals in stage 0 was subtracted from tau PET SUVR in individual regions of interest. A35 = Brodmann area 35; A36 = Brodmann area 36; Aβ = amyloid-β; CU = cognitively unimpaired; ERC = entorhinal cortex; IPC = inferior parietal cortex; ITC = inferior temporal cortex; MTC = middle temporal cortex; PHC = parahippocampal cortex; PRE = precuneus; RSC = retrosplenial cortex.

Spatial distribution of tau accumulation in early disease stages

With the aim to visualize the spatial distribution of tau accumulation in different tau-EBM stages, we followed a voxel-wise approach and grouped individuals in different stage groups (Fig. 1B). Individuals in EBM stages 1–3 were mostly characterized by

tau-PET binding in Brodmann area 35 and the entorhinal cortex (Fig. 2A). In addition, there were two bilateral clusters in the subiculum and cornu ammonis (CA) 1, which are in line with early depictions of Braak stages I–II in the neuropathological literature[8] and correspond roughly to the prosubiculum.[10,40,41] Notably, we also observed significant tau-PET binding in the amygdala, which
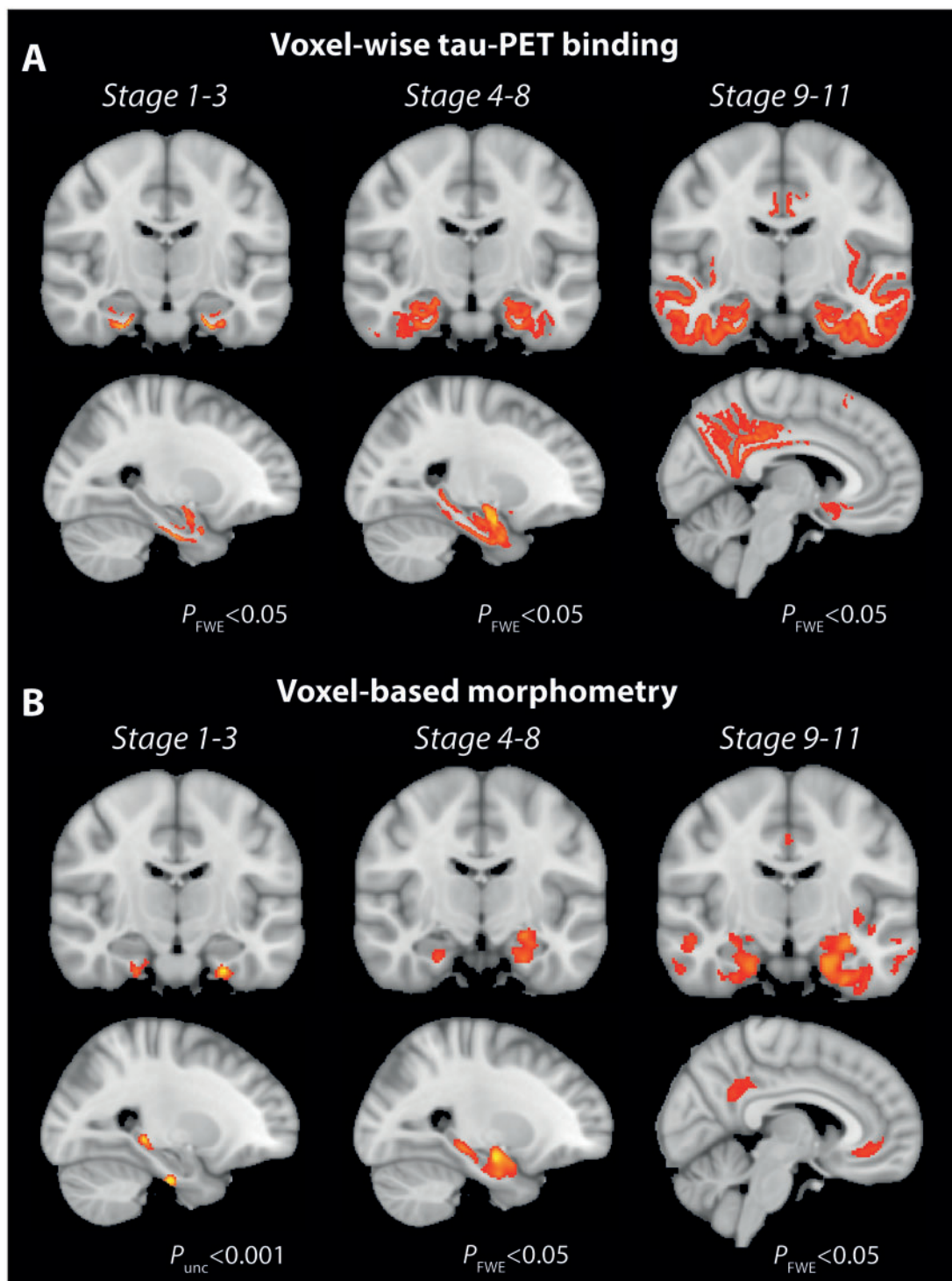
Figure 2 Voxel-wise tau-PET binding and voxel-based morphometry across tau-EBM stages. (**A**) Voxel-wise group differences in tau-PET SUVR images resulting from two-sample *t*-tests between a group corresponding to tau-EBM stage 0 (*n* = 281) and groups corresponding to stage 1–3 (*n* = 35), stage 4–8 (*n* = 29) and stage 9–11 (*n* = 38), respectively. (**B**) Group differences derived from voxel-based morphometry between identical groups. Voxel-wise results in all analyses were corrected using family-wise error (FWE) correction at a threshold of *P* < 0.05 and a cluster size of 50 mm^3. The voxel-based morphometry group comparison between individuals in stage 1–3 and individuals in stage 0 (**B**, *left*) did not yield significant results using that statistical threshold and is thus reported at an uncorrected threshold of *P* < 0.001.

can be appreciated in the sagittal view in Fig. 2A. Individuals in tau-EBM stages 4–8 show additional tau-PET binding in the posterior hippocampus (mostly subiculum/CA1 or prosubiculum), more widespread accumulation in the anterior hippocampus and extended neocortical temporal accumulation (e.g. Brodmann area

36 and parahippocampal cortex) (Fig. 2A). Thus, tau pathology seems to accumulate predominantly in anterior MTL regions in the beginning before it progresses more posteriorly and to lateral temporal regions, in line with our region of interest-based results displayed in Fig. 1D. Finally, tau-EBM stages 9–11 were

characterized by even stronger tau accumulation in lateral temporal brain regions as well as middle parietal and orbitofrontal brain regions (Fig. 2A). Voxel-wise results are available as videos going through all posterior-anterior brain slices in the Supplementary material. Peak cluster coordinates can be found in Supplementary Tables 1–3.

MTL subregional tau is related to local and distant subregional atrophy in cognitively unimpaired individuals

Next, we were interested in whether tau accumulation in MTL subregions was associated with subregional atrophy. Analyses were carried out separately in cognitively unimpaired individuals and patients with MCI to investigate disease stage-specific relationships. Based on our previous finding that cognitively unimpaired individuals were almost entirely restricted to stages where tau deposition was limited to MTL subregions (mostly in tau-EBM stages <7), we focused on relationships between tau deposition and atrophy of MTL subregions. Using linear regression models, we found two types of relationships. Local relationships where tau in a given MTL subregion was associated with atrophy of the same region (Fig. 3A, diagonal highlighted in blue) were observed for the entorhinal cortex, Brodmann area 35 and the anterior and posterior hippocampus (Fig. 3)—subregions that were the earliest in the sequence identified by the EBM (Fig. 1D). We also found distant effects where tau in one region was associated with atrophy in a distant region. Here, tau in all MTL subregions—except the parahippocampal cortex—was related to posterior hippocampal atrophy. In MCI patients, we found a local effect of tau on atrophy in the posterior hippocampus (Fig. 3B, $P_{FDR} < 0.005$). All models were corrected for continuous cortical amyloid-β PET levels (see Supplementary material for uncorrected analyses). Amyloid-β PET levels were not associated with cortical thickness or volume of

most MTL subregions (even when not accounting for tau-PET) in cognitively unimpaired individuals (all P_{FDR} values > 0.5) and MCI patients (all P_{FDR} > 0.14), except for posterior hippocampal volume [MCI: β = −251, standard error (SE) = 88.2, P_{FDR} = 0.03; trend in cognitively unimpaired individuals: β = −103.7, SE = 41.8, P_{FDR} = 0.08].

Finally, we used voxel-based morphometry to analyse volumetric differences between all three stage groups derived from the EBM on a whole-brain level by contrasting them against individuals in stage 0. We found no differences in the earliest stages 1–3, but clear differences in stages 4–8 and 9–11. While atrophy in stages 4–8 was limited to the MTL (Fig. 2B and Supplementary Table 4), there was more widespread atrophy in stages 9–11, including more neocortical temporal regions as well as medial and lateral parietal and frontal brain regions (Fig. 2B and Supplementary Table 5). These results largely mirrored our stage-specific voxel-wise tau-PET binding patterns (Fig. 2A). Importantly, while we did not find differences in the earliest group in stages 1–3 at a corrected statistical threshold ($P_{FWE} < 0.05$), we found a convincing pattern at an uncorrected threshold ($P < 0.001$). With evident tau binding in anterior MTL regions, atrophy was limited to Brodmann area 35 (transentorhinal region), the lateral portion of the entorhinal cortex and the posterior hippocampus (Fig. 2B). Although at an uncorrected threshold, these results mirror our region of interest-based finding arguing for the presence of early posterior hippocampal atrophy in the absence of measurable local tau accumulation.

MTL atrophy is related to memory performance in MCI patients, but not cognitively unimpaired individuals

Next, we were interested in how MTL subregional tau and atrophy are related to memory performance in cognitively unimpaired individuals. Following multiple comparisons correction, we found
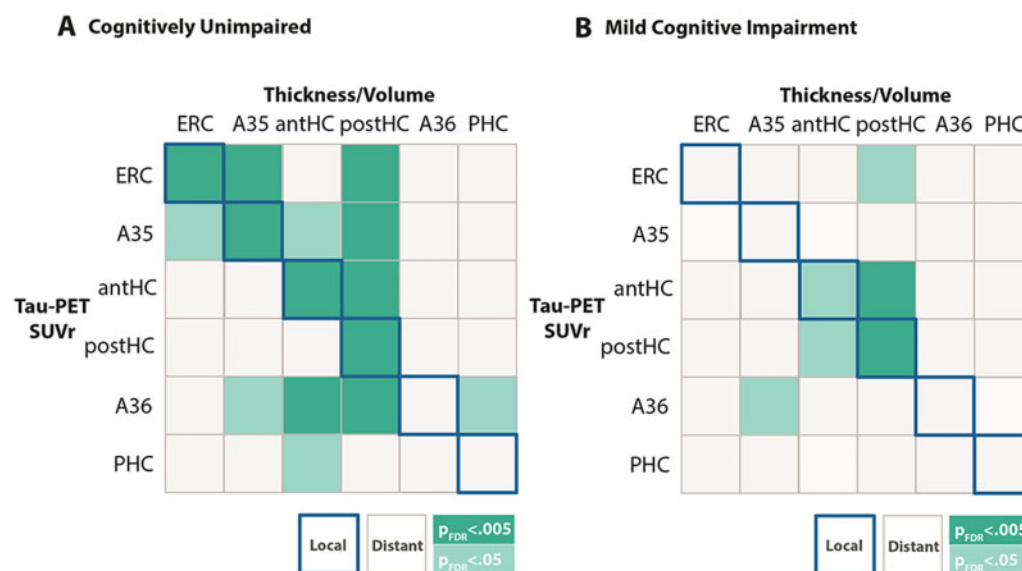

Figure 3 Relationship between MTL subregional tau SUVR and atrophy. (A) Relationships in cognitively unimpaired individuals and (B) in patients with MCI. Correlation matrices show the relationship between subregional measures of tau SUVR (rows) and atrophy measures (columns). Relationships lying on the diagonal (highlighted in blue) indicate local relationships between a given subregions tau SUVR and local thickness or volume. Relationships off the diagonal indicate distant effects, where tau SUVR in one region was associated with atrophy in another region. Dark green represents multiple regression models that are significant at $P_{FDR} < 0.005$, while light green indicate significance at $P_{FDR} < 0.05$. All regression models were corrected for age, sex and continuous amyloid-β PET SUVR in the cortical composite region. Regression models including volumetric measures (anterior and posterior hippocampus) were additionally corrected for intracranial volume. A35 = Brodmann area 35; A36 = Brodmann area 36; Aβ = amyloid-β; CU = cognitively unimpaired; ERC = entorhinal cortex; IPC = inferior parietal cortex; ITC = inferior temporal cortex; MTC = middle temporal cortex; PHC = parahippocampal cortex; PRE = precuneus; RSC = retrosplenial cortex.

that tau-PET SUVR in entorhinal cortex, Brodmann area 35 and anterior hippocampus was associated with delayed word recall performance (entorhinal: $\beta = 0.73$, SE = 0.27, $P_{FDR} = 0.017$; Brodmann area 35: $\beta = 0.9$, SE = 0.34, $P_{FDR} = 0.017$; anterior hippocampus: $\beta = 2.16$, SE = 0.7, $P_{FDR} = 0.014$) (Fig. 4A). All relationships also survived multiple comparison correction after applying robust regression models. However, there were no significant relationships between memory performance and volume/thickness of any MTL subregions (all P-values > 0.6; Fig. 4B). While cortical amyloid-β PET SUVR was associated with memory performance ($\beta = 0.98$, SE = 0.39, $P = 0.012$), a mediation analysis showed that tau-PET binding in Brodmann area 35, entorhinal cortex and anterior hippocampus each significantly and fully mediated the effect of amyloid-β PET on memory, leaving no additional significant direct effect [Brodmann area 35: $\beta = 0.112$ (0.029–0.195), $P = 0.008$; entorhinal: $\beta = 0.125$ (0.036–0.215), $P = 0.006$; anterior hippocampus: $\beta = 0.098$ (0.025–0.170), $P = 0.008$].

To compare early effects of tau accumulation on MTL atrophy and memory functioning with later disease stages, we conducted the same analysis in the amyloid-β+ MCI patients. While tau accumulation in the anterior and posterior hippocampus was related to memory (anterior hippocampus: $\beta = 2.47$, SE = 0.75, $P_{FDR} = 0.004$; posterior hippocampus: $\beta = 3.7$, SE = 0.96, $P_{FDR} = 0.001$) (Fig. 4C), we observed statistical trends in Brodmann area 35 and the entorhinal cortex ($P_{FDR} = 0.051$ and $P_{FDR} = 0.077$, respectively). Furthermore, posterior hippocampal atrophy was significantly related to memory performance ($\beta = -0.003$, SE = 0.00096, $P_{FDR} = 0.009$) (Fig. 4D). Mediation analyses showed that posterior hippocampal atrophy mediated the effect of anterior hippocampal tau on memory performance [$\beta = 0.105$ (0.002–0.207), $P = 0.049$] (Fig. 4E and F) and showed a trend for a mediation of the effect of posterior hippocampal tau on memory performance [$\beta = 0.09$ (–0.005 to 0.184), $P = 0.063$]. In both mediation analyses, there remained a significant direct effect of tau on memory performance. Again, amyloid-β PET SUVR was associated with memory performance ($\beta = 0.4$, SE = 0.1, $P = 0.0001$) and a mediation analysis confirmed that anterior [$\beta = 0.145$ (0.039–0.252), $P = 0.007$] and posterior hippocampal tau [$\beta = 0.105$ (0.013–0.197), $P = 0.025$] significantly mediated the effect of amyloid-β PET on memory to a large extent, but there remained a direct effect of amyloid-β PET on memory.

Tau accumulation disrupts MTL-cortical functional connectivity

Our findings point towards a role of Brodmann area 35, entorhinal and anterior hippocampal tau pathology in memory impairment for cognitively unimpaired older adults while hippocampal tau pathology and posterior hippocampal atrophy were associated with memory impairment in MCI patients. We have recently reported that changes in functional connectivity between the MTL (especially entorhinal cortex and Brodmann area 35) and regions in the anterior-temporal and posterior-medial system seemingly preceded significant atrophy in cognitively unimpaired individuals.[16] Given that measures of atrophy were not associated with memory performance in cognitively unimpaired individuals in the present study, we were interested in how functional connectivity between the MTL and cortical memory systems changes with increasing Brodmann area 35 and entorhinal tau-PET signal. We found decreased functional connectivity between areas 35 and 36, entorhinal cortex and the anterior hippocampus on the one hand, and regions in the anterior-temporal system (mostly temporal pole, medial prefrontal and orbitofrontal cortex) on the other hand (Fig. 5A and B). While this represents functional connectivity networks that were significantly reduced with increasing tau-PET signal in Brodmann area 35 and entorhinal cortex, reduced

connectivity across both components was not significantly associated with memory performance (Brodmann area 35 tau SUVR: $\beta = -0.019$, SE = 0.016, $P = 0.223$; entorhinal tau SUVR: $\beta = -0.03$, SE = 0.04, $P = 0.467$). To identify the subset of links in the network component that are both reduced with increasing tau pathology and relevant to memory performance, we identified three subcomponents (Fig. 5C) correlating with memory performance. These subcomponents consisted of reduced functional connectivity between (i) Brodmann area 35 and the orbitofrontal/medial prefrontal cortex; (ii) the posterior hippocampus, the parahippocampal cortex and the angular gyrus; as well as (iii) between the entorhinal cortex, anterior hippocampus and the posterior cingulate cortex (including the retrosplenial cortex) (Fig. 5C).

Discussion

Using a second generation tau-PET tracer, detailed subdivision of MTL subregions and EBM, we identified the sequence of tau progression across the MTL and the posterior-medial system in Alzheimer's disease. The entorhinal cortex and Brodmann area 35 (i.e. transentorhinal region) were affected very early by tau pathology and showed the steepest increase in tau-PET signal in early disease stages. Other MTL subregions, such as the hippocampus, Brodmann area 36 and parahippocampal cortex followed, before middle and inferior temporal and inferior parietal regions, retrosplenial cortex and precuneus became abnormal. In cognitively unimpaired individuals, tau accumulation was mostly limited to MTL subregions. Atrophy mirrored the spatial distribution pattern of tau-PET binding with the notable exception of early posterior hippocampal atrophy. While tau-PET binding was tightly associated with MTL subregional atrophy, only tau in Brodmann area 35, entorhinal cortex and the anterior hippocampus was related to memory performance. Importantly, no measure of grey matter volume or thickness was associated with memory performance in cognitively unimpaired individuals. In contrast, tau-PET binding in the hippocampus, as well as posterior hippocampal atrophy, were both strongly associated with memory in MCI patients. Mediation analyses revealed that atrophy mediated the effect of tau pathology on memory. Finally, functional connectivity analyses revealed that transentorhinal tau pathology in cognitively unimpaired individuals resulted primarily in reduced MTL–anterior-temporal functional connectivity. Meanwhile, tau-related reductions in functional connectivity in critical MTL–posterior-medial networks were associated with early subtle memory impairment.

Early locus of tau-PET binding in the MTL using a second generation tracer resembles neuropathological findings

The neuropathological literature suggests the earliest cortical neurofibrillary tau tangles accumulate in an area in the anterior MTL that covers the transentorhinal region and part of the entorhinal cortex.[8,10] Following the first stage of Braak's staging scheme, tau tangles increase in number in Brodmann area 35 and the entorhinal cortex and can be detected in CA1 in Braak stage II, however, in a region adjacent to the subiculum, which roughly matches a region referred to as the prosubiculum.[10,40,41] While neurofibrillary tangle counts increase in the mentioned subregions in stage III/IV, they can also be found in lower numbers in other hippocampal subfields and more lateral temporal regions such as Brodmann area 36. Finally, in Braak stages V/VI, tau pathology can be found in neocortical association cortices.

Using tau-PET imaging with a second generation tracer that allows more accurate measurement of hippocampal tau-PET binding, our results are in line with Braak and Braak's findings of the earliest tau accumulation in the entorhinal cortex, Brodmann area
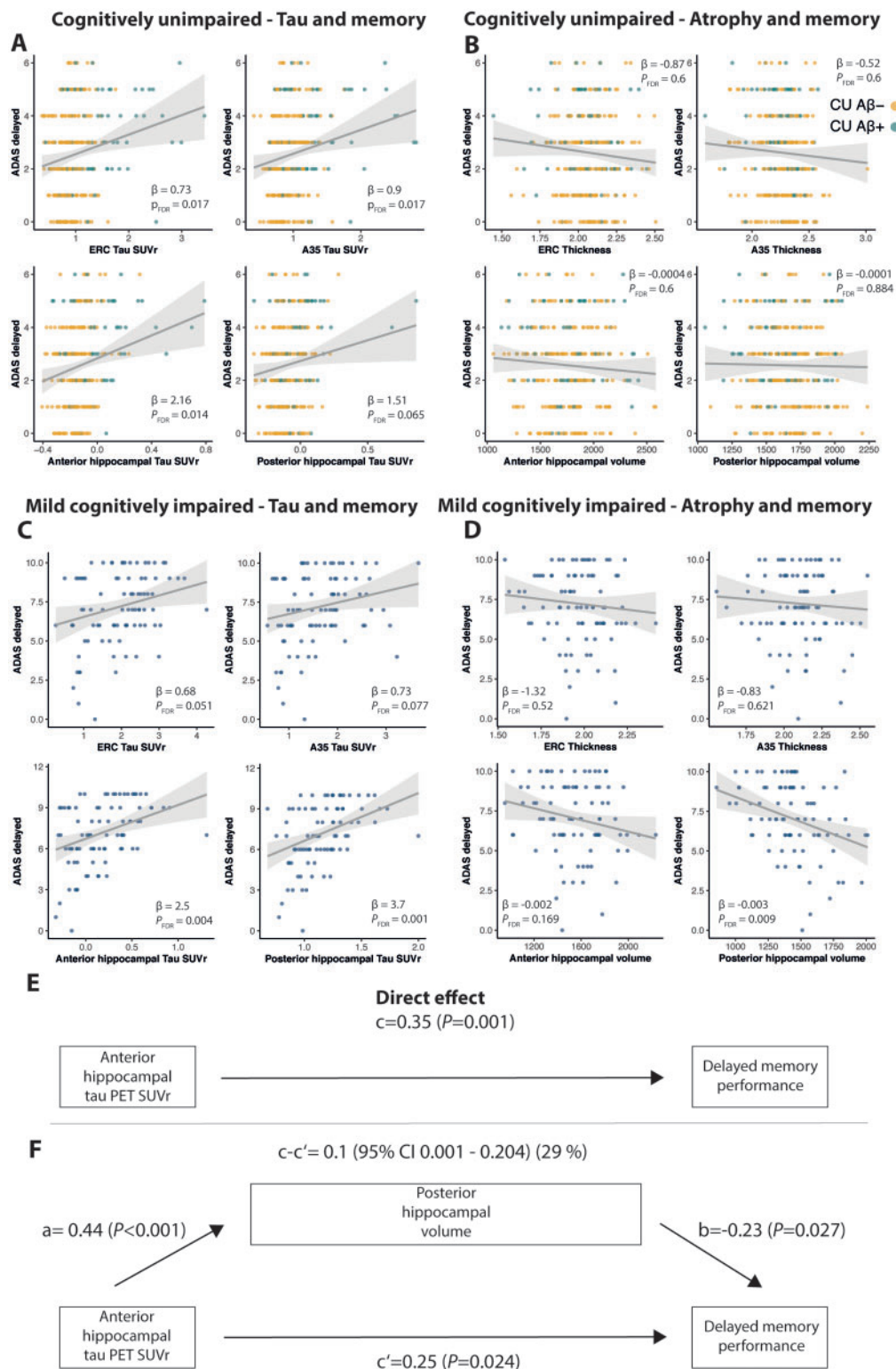
Figure 4 Relationships between MTL tau SUVR, memory performance and atrophy in cognitively unimpaired individuals and patients with MCI. Relationships between MTL tau SUVR and memory in (**A**) cognitively unimpaired and (**C**) MCI as well as between MTL atrophy and memory in (**B**) cognitively unimpaired and (**D**) MCI. A mediation analysis revealed that posterior hippocampal volume partially mediates the relationship between anterior hippocampal tau SUVR and memory. (**E**) The direct effect (c) of anterior hippocampal tau SUVR on delayed memory performance. (**F**) The mediated effect of posterior hippocampal volume is designated c-c′. The remaining effect of anterior hippocampal tau SUVR on delayed memory performance after adjusting for posterior hippocampal volume is designated 'c''. The direct effect of anterior hippocampal tau-PET SUVR on posterior hippocampal volume is 'a', the effect of posterior hippocampal volume on delayed memory performance is 'b'. All regression models were corrected for age, sex, years of education and continuous amyloid-β PET SUVR in a cortical composite region. Regression models including volumetric measures (anterior and posterior hippocampus) were additionally corrected for intracranial volume. Note that ADAS delayed recall performance is reported in number of errors. A35 = Brodmann area 35; ERC = entorhinal cortex.
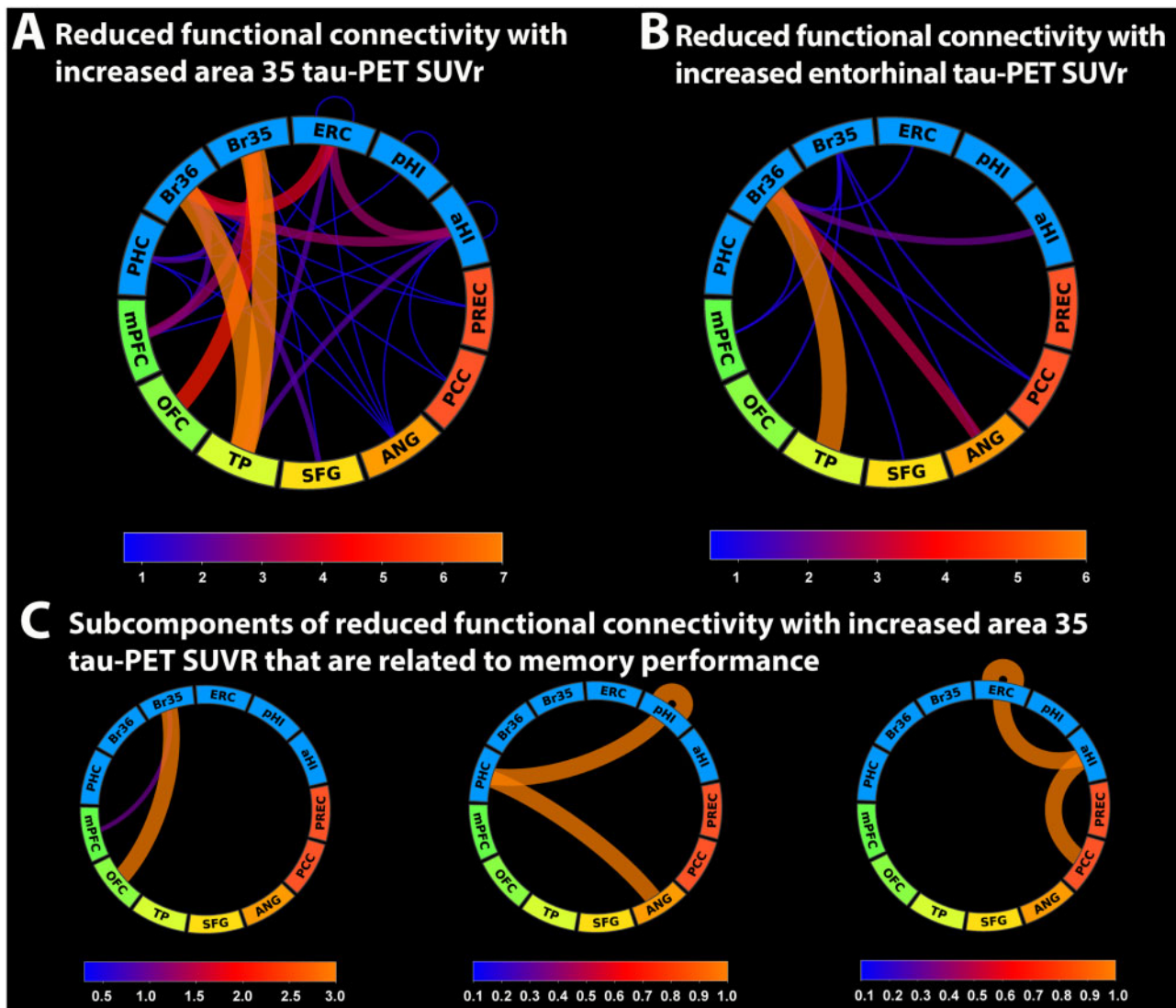
Figure 5 Changes in functional connectivity between the MTL and regions in the anterior-temporal and posterior-medial system in cognitively unimpaired individuals. (**A**) Network component of reduced functional connectivity with increasing tau-PET signal in Brodmann area 35 and (**B**) the entorhinal cortex. (**C**) Subcomponents of **A** that are significantly associated to delayed recall memory performance. Line width and colour in the connectograms are proportional to the number of links between regions of interest as indicated in the corresponding scale. A35 = Brodmann area 35; A36 = Brodmann area 36; Aβ = amyloid-β; CU = cognitively unimpaired; ERC = entorhinal cortex; IPC = inferior parietal cortex; ITC = inferior temporal cortex; MTC = middle temporal cortex; PHC = parahippocampal cortex; PRE = precuneus; RSC = retrosplenial cortex.

35 and the anterior hippocampus. Our voxel-wise results show an almost exact replication of their original findings where tau-PET binding could be observed in a region spanning Brodmann area 35 (i.e. transentorhinal region), entorhinal cortex and an area in the anterior hippocampus consistent with boundaries of CA1 with the subiculum, roughly matching prosubiculum. This is also in line with a recent autopsy imaging study combining *ex vivo* MRI and serial histopathology, which identified an almost identical pattern,[42] as well as a study showing that Braak stage was associated with neuron loss in the subicular end of CA1.[43] We also found consistent tau-PET signal in the amygdala early on, congruent with earlier studies.[44,45] In later stages, tau binding was detected in other temporal cortical regions such as Brodmann area 36, again consistent with Braak and Braak's findings. While tau-PET binding could be observed in early stages in the anterior MTL, binding in later stages was seen in the subiculum/CA1 of the posterior hippocampus and in the parahippocampal cortex. These findings

suggest that specific regions in the posterior MTL are affected in later disease stages. Hippocampal tau-PET signal never reached the levels of neocortical regions. One underlying reason might be that tau pathology is particularly accumulating in subiculum and CA1 while other subregions, such as CA2–3 and the dentate gyrus, seem rather spared in non-demented individuals (Supplementary Videos 1–3). Given that we report the mean signal of all voxels in the anterior/posterior hippocampus, the mean tau-PET signal is likely lower on average compared to cortical regions.

Taken together, we found the earliest signs of abnormal tau-PET signal in regions of the anterior-temporal system while progressively more regions of the posterior-medial system became abnormal in later tau-EBM stages.[4,46] As it is likely that the nature of cognitive and particularly memory impairment will change depending on the spatial distribution of tau pathology in functional memory systems. These findings can inform research on disease stage-specific cognitive markers.[46]

Medial temporal tau is locally and remotely associated with grey matter atrophy

Tau binding has recently been shown to be tightly linked to atrophy.[2,13,15] In line with these earlier findings, our voxel-based morphometry results across different tau-EBM stages showed a very similar atrophy pattern compared to voxel-wise tau-PET binding. In addition, our region of interest analysis revealed that tau pathology was associated with local thickness and volume within regions such as the entorhinal cortex, Brodmann area 35 and the hippocampus. This is congruent with earlier studies that reported cross-sectional and longitudinal atrophy in MTL subregions associated with MTL tau-PET binding.[14,47,48] However, while earlier studies collapsed across amyloid-β+ participants, including cognitively unimpaired, MCI and Alzheimer's disease patients, we show in a larger sample that anterior MTL tau-PET binding is associated with atrophy already in cognitively unimpaired individuals. In addition, while earlier studies used an MTL-tau composite, we used tau-PET signal from individual regions of interest, and the reduced off-target binding of ^{18}F-RO948 tau-PET allowed us to analyse the signal from the hippocampus.[17] With this approach, we could separate local and distant relationships between tau accumulation and atrophy.

In addition to local relationships, we found a robust effect where tau in distant MTL subregions was strongly associated with lower volume of the posterior hippocampus, suggesting remote mechanisms of atrophy in addition to local effects. This finding was additionally confirmed by our voxel-based morphometry analysis. The relationship between primarily posterior hippocampal atrophy and tau pathology has recently been reported in several studies. De Flores and colleagues[49] reported that tau pathology, measured as a mean score of tau tangles in entorhinal cortex, subiculum and CA1, was associated with ante-mortem posterior hippocampal volume and Xie and colleagues[50] reported the earliest longitudinal decline in preclinical Alzheimer's disease in Brodmann area 35 and the posterior hippocampus. Furthermore, a study from our group showed additional evidence for lower posterior hippocampal volume of the subiculum with increased levels of CSF p-Tau.[51] In sum, while earlier studies have shown consistent local relationships between tau and MTL atrophy, our findings extend these by revealing early tau-related atrophy of the posterior hippocampus *in vivo* that likely results from distant rather than local mechanisms. While we can only speculate on the underlying mechanisms, it is interesting that anterior-lateral regions in the entorhinal cortex neighbouring the collateral sulcus and Brodmann area 35, receive mostly projections from the posterior hippocampus (CA1/subiculum).[52] The same region shows the earliest tau-related atrophy,[42] suggesting that posterior hippocampal atrophy could be driven by a loss of connections between the anterior-lateral entorhinal cortex and the posterior hippocampus.

Tau and functional connectivity, but not atrophy, are associated with memory performance in cognitively unimpaired individuals

Earlier work has suggested a tight link between tau, neurodegeneration and cognitive performance.[1,2,13] Here we extend that literature with a fine-grained anatomical analysis. We show that entorhinal, Brodmann area 35 and anterior hippocampal tau-PET binding were related to memory performance in cognitively unimpaired individuals, while only hippocampal tau-PET binding was associated with memory in MCI patients. Critically, while memory was not associated with atrophy in any MTL region in the cognitively unimpaired, posterior hippocampal atrophy mediated the effect of hippocampal tau on memory in MCI patients. Taken together, this suggests that while tau-related memory impairment might be less dependent on atrophy in early disease stages, it seems to depend on posterior hippocampal atrophy at the MCI stage. Recent work using lesion mapping further strengthens the role of the posterior hippocampus in memory impairment showing that lesions causing amnesia were all functionally connected to an area spanning the posterior hippocampus and parts of the retrosplenial cortex.[53] In light of these findings, our results suggest that memory impairment in Alzheimer's disease becomes fully evident once the posterior hippocampus, as the core region of an episodic memory circuit, is affected by atrophy. Whether there is a qualitative difference between subtle tau-related memory impairment in cognitively unimpaired individuals and tau- and atrophy-related impairment in MCI patients needs to be addressed in future studies using several different memory measures.

We have recently reported changes in functional connectivity between the MTL and regions in the anterior-temporal/posterior-medial system in different stages of Alzheimer's disease.[16] While there was primarily reduced MTL-anterior-temporal connectivity in early disease stages (CU amyloid-β+ versus CU amyloid-β–), predominant reductions in MTL-posterior-medial functional connectivity characterized individuals in later disease stages (amyloid-β+ MCI patients versus CU amyloid-β–). In addition, reduced MTL-posterior-medial functional connectivity was more consistently associated with memory impairment. In line with these earlier results, the findings of our present study show that increases in tau-PET signal in the transentorhinal and entorhinal region in cognitively unimpaired individuals were mainly associated with reduced MTL-anterior-temporal functional connectivity. This is in agreement with a recent study that reported a hippocampus-anterior-temporal system disconnection, paired with increased regional hippocampal homogeneity, to be associated with increasing MTL tau-PET signal.[54] While these recent results, as well our analyses, point towards a predominant tau-related MTL-anterior-temporal disconnection, results from our subcomponent analysis suggest that functional connectivity within critical MTL-posterior-medial networks connecting the entorhinal cortex, hippocampus, parahippocampal cortex, angular gyrus and the posterior cingulate/retrosplenial cortex is particularly associated with tau-related verbal memory impairment. These resulting subcomponents are congruent with recent reports highlighting functional connectivity between the MTL and parietal nodes of the default mode network to be particularly relevant for episodic memory.[53,55] While we could identify subnetworks that are particularly vulnerable to early tau accumulation and were associated with memory impairment, our data-driven analysis approach does not allow us to test to what degree these changes in functional connectivity can explain tau-related memory impairment. Future studies focusing on the interactions of specific functional connectivity networks, tau pathology and memory function in independent cohorts of cognitively unimpaired individuals are needed.

Limitations

First, our identified order of biomarker abnormality in tau-PET SUVR across different subregions is based on cross-sectional measurements instead of longitudinal data. Second, the implementation of the EBM used here assumes one common trajectory for participants. While this might be true, there could still be individuals with non-typical spread of tau.[56] Third, while our overall sample consists of 383 individuals, groups of individual stages were not large enough to carry out individual stage-specific analyses, requiring us to collapse across stages. Fourth, while we followed a unique approach using individually derived fine-grained MTL subregions, the resulting regions of interest were in part quite

small and challenge the resolution offered by tau-PET. However, even the Brodmann area 35 region of interest in our study has a volume of 1202 ± 204 mm^3 (mean $\pm$ SD); resulting in ~10 voxels in the tau-PET resolution. Fifth, while the tau-PET tracer in our study showed considerably reduced off-target binding in the choroid plexus,[17] tau tracers with even lower choroid plexus binding may be better suited for assessing MTL subregions. Finally, we used ADAS-delayed 10-word recall as a measure of memory performance, which limits our results to a specific memory measure. Given the specificity of tau-related effects on atrophy and functional connectivity in different disease stages, future studies with several different and more specific memory measures are needed to further understand the nature of early tau-related memory impairment.

Conclusion

Taken together, our findings provide an anatomically detailed insight into tau progression across fine-grained MTL subregions and memory-relevant cortical regions in non-demented individuals. While tau pathology might affect memory performance in cognitively unimpaired individuals via reduced functional connectivity in critical MTL-cortical networks, memory impairment in MCI seems to be associated with posterior hippocampal atrophy.

Acknowledgements

We want to thank all participants of the Swedish BioFINDER-2 study and their families for their participation in the study. We also want to thank Oisín Clancy and Hannah Baumeister for their help with the manual quality assessment of the medial temporal subregional masks.

Competing interests

O.H. has acquired research support (for the institution) from AVID Radiopharmaceuticals, Biogen, Eli Lilly, Eisai, GE Healthcare, Pfizer, and Roche. In the past 2 years, he has received consultancy/speaker fees from AC Immune, Alzpath, Biogen, Cerveau and Roche. The other authors report no competing interests.

Supplementary material

Supplementary material is available at *Brain* online.

References

1. Nelson PT, Alafuzoff I, Bigio EH, et al. Correlation of Alzheimer disease neuropathologic changes with cognitive status: A review of the literature. *J Neuropathol Exper Neurol.* 2012;71(5): 362–381.
2. Maass A, Lockhart SN, Harrison TM, et al. Entorhinal tau pathology, episodic memory decline, and neurodegeneration in aging. *J Neurosci.* 2018;38(3):530–543.
3. Ritchey M, Libby LA, Ranganath C. Progress in brain research. *Progr Brain Res.* 2015;219:45–64.
4. Ranganath C, Ritchey M. Two cortical systems for memory-guided behaviour. *Nat Rev Neurosci.* 2012;13(10):713–726.
5. Palmqvist S, Schöll M, Strandberg O, et al. Earliest accumulation of amyloid-β occurs within the default-mode network and concurrently affects brain connectivity. *Nat Commun.* 2017;8(1): 1214.
6. Mattsson N, Palmqvist S, Stomrud E, Vogel J, Hansson O. Staging β-amyloid pathology with amyloid positron emission tomography. *JAMA Neurol.* 2019;76(11):1319.
7. Maass A, Berron D, Harrison TM, et al. Alzheimer's pathology targets distinct memory networks in the ageing brain. *Brain.* 2019;142(8):2492–2509.
8. Braak H, Braak E. Staging of Alzheimer's disease-related neurofibrillary changes. *Neurobiol Aging.* 1995;16(3):271–278.
9. Schöll M, Lockhart SN, Schonhaut DR, et al. PET imaging of tau deposition in the aging human brain. *Neuron.* 2016;89(5): 971–982.
10. Braak H, Tredici KD. From the entorhinal region via the prosubiculum to the dentate fascia: Alzheimer disease-related neurofibrillary changes in the temporal allocortex. *J Neuropathol Exper Neurol.* 2020;79(2):163–175.
11. Pascoal TA, Therriault J, Benedet AL, et al. 18F-MK-6240 PET for early and late detection of neurofibrillary tangles. *Brain.* 2020; 143(9):2818–2830.
12. Ossenkoppele R, Rabinovici GD, Smith R, et al. Discriminative accuracy of [18 F]flortaucipir positron emission tomography for Alzheimer disease vs other neurodegenerative disorders. *JAMA.* 2018;320(11):1151.
13. Bejanin A, Schonhaut DR, Joie R, et al. Tau pathology and neurodegeneration contribute to cognitive impairment in Alzheimer's disease. *Brain.* 2017;140(12):3286–3300.
14. Xie L, Das SR, Wisse L, et al.; Alzheimer's Disease Neuroimaging Initiative. Early tau burden correlates with higher rate of atrophy in transentorhinal cortex. *J Alzheimers Dis.* 2018;62(1):85–92.
15. Joie RL, Visani AV, Baker SL, et al. Prospective longitudinal atrophy in Alzheimer's disease correlates with the intensity and topography of baseline tau-PET. *Sci Transl Med.* 2020;12(524): eaau5732.
16. Berron D, van Westen D, Ossenkoppele R, Strandberg O, Hansson O. Medial temporal lobe connectivity and its associations with cognition in early Alzheimer's disease. *Brain.* 2020; 143(4):1233–1248.
17. Smith R, Schöll M, Leuzy A, et al. Head-to-head comparison of tau positron emission tomography tracers [18F]flortaucipir and [18F]RO948. *Eur J Nucl Med Mol Imaging.* 2020;47(2):342–313.
18. Young AL, Oxtoby NP, Daga P, et al. A data-driven model of biomarker changes in sporadic Alzheimer's disease. *Brain.* 2014; 137(9):2564–2577.
19. Xie L, Wisse LEME, Pluta J, et al.; for the Alzheimer's Disease Neuroimaging Initiative. Automated segmentation of medial temporal lobe subregions on in vivo T1-weighted MRI in early stages of Alzheimer's disease. *Hum Brain Mapping.* 2019;40(12): 3431–3451.

20. Cho SH, Choe YS, Park S, et al. Appropriate reference region selection of 18F-florbetaben and 18F-flutemetamol beta-amyloid PET expressed in Centiloid. *Sci Rep*. 2020;10(1):14950.

21. Xie L, Pluta JB, Das SR, et al. Multi-template analysis of human perirhinal cortex in brain MRI: Explicitly accounting for anatomical variability. *Neuroimage*. 2017;144(Pt A):183–202.

22. Baker SL, Maass A, Jagust WJ. Considerations and code for partial volume correcting [18F]-AV-1451 tau PET data. *Data Brief*. 2017;15(Acta Neuropathol):648–657.

23. Rousset OG, Ma Y, Evans AC. Correction for partial volume effects in PET: Principle and validation. *J Nucl Med*. 1998;39(5):904–911.

24. Thomas BA, Erlandsson K, Modat M, et al. The importance of appropriate partial volume correction for PET quantification in Alzheimer's disease. *Eur J Nucl Med Mol*. 2011;38(6):1104–1119.

25. Thurfjell L, Lilja J, Lundqvist R, et al. Automated quantification of 18F-flutemetamol PET activity for categorizing scans as negative or positive for brain amyloid: Concordance with visual image reads. *J Nucl Med*. 2014;55(10):1623–1628.

26. Fonteijn HM, Modat M, Clarkson MJ, et al. An event-based model for disease progression and its application in familial Alzheimer's disease and Huntington's disease. *Neuroimage*. 2012;60(3):1880–1889.

27. Vogel JW, Iturria-Medina Y, Strandberg OT, et al.; Swedish BioFinder Study. Spread of pathological tau proteins through communicating neurons in human Alzheimer's disease. *Nat Commun*. 2020;11(1):2612.

28. Avants BB, Tustison NJ, Stauffer M, Song G, Wu B, Gee JC. The Insight ToolKit image registration framework. *Front Neuroinform*. 2014;8:44.

29. Ashburner J. A fast diffeomorphic image registration algorithm. *Neuroimage*. 2007;38(1):95–113.

30. Jenkinson M, Beckmann CF, Behrens TE, Woolrich MW, Smith SM. FSL. *Neuroimage*. 2012;62(2):782–790.

31. Cox RW. AFNI: Software for analysis and visualization of functional magnetic resonance neuroimages. *Comput Biomed Res Int J*. 1996;29(3):162–173.

32. Grabner G, Janke AL, Budge MM, Smith D, Pruessner J, Collins DL. Symmetric atlasing and model based segmentation: An application to the hippocampus in older adults. *Med Image Comput Comp Assist Interv*. 2006;9(Pt 2):58–66.

33. Behzadi Y, Restom K, Liau J, Liu TT. A component based noise correction method (CompCor) for BOLD and perfusion based fMRI. *NeuroImage*. 2007;37(1):90–101.

34. Friston KJ, Williams S, Howard R, Frackowiak RSJ, Turner R. Movement-related effects in fMRI time-series. *Magnet Reson Med*. 1996;35(3):346–355.

35. Wang S, Peterson DJ, Gatenby JC, Li W, Grabowski TJ, Madhyastha TM. Evaluation of field map and nonlinear registration methods for correction of susceptibility artifacts in diffusion MRI. *Front Neuroinform*. 2017;11:17.

36. Power JD, Barnes KA, Snyder AZ, Schlaggar BL, Petersen SE. Spurious but systematic correlations in functional connectivity MRI networks arise from subject motion. *Neuroimage*. 2012;59(3):2142–2154.

37. Fan L, Li H, Zhuo J, et al. The human brainnetome atlas: A new brain atlas based on connectional architecture. *Cereb Cortex*. 2016;26(8):3508–3526.

38. Rosen WG, Mohs RC, Davis KL. A new rating scale for Alzheimer's disease. *Am J Psychiatry*. 1984;141(11):1356–1364.

39. Rosseel Y. lavaan: An R Package for Structural Equation Modeling. *J Stat Softw*. 2012;48(2):1–36. doi:10.18637/jss.v048.i02

40. Schönheit B, Zarski R, Ohm TG. Spatial and temporal relationships between plaques and tangles in Alzheimer-pathology. *Neurobiol Aging*. 2004;25(6):697–711.

41. Lace G, Savva GM, Forster G, et al. Hippocampal tau pathology is related to neuroanatomical connections: An ageing population-based study. *Brain*. 2009;132(5):1324–1334.

42. Ravikumar S, Wisse LEM, Ittyerah R et al. Building an Ex Vivo Atlas of the Earliest Brain Regions Affected by Alzheimer's Disease Pathology. In: *2020 IEEE 17th International Symposium on Biomedical Imaging*. 2020:113–117.

43. Hokkanen SRK, Hunter S, Polvikoski TM, et al.; MRC CFAS and CC75C Study Group. Hippocampal sclerosis, hippocampal neuron loss patterns and TDP-43 in the aged population: Population-based hippocampal neuron loss. *Brain Pathol*. 2018;28(4):548–559.

44. Insel PS, Mormino EC, Aisen PS, Thompson WK, Donohue MC. Neuroanatomical spread of amyloid β and tau in Alzheimer's disease: Implications for primary prevention. *Brain Commun*. 2020;2(1):fcaa007.

45. Vogt LJK, Hyman BT, Hoesen GWV, Damasio AR. Pathological alterations in the amygdala in Alzheimer's disease. *Neurosci*. 1990;37(2):377–385.

46. Ritchey M, Cooper RA. Deconstructing the posterior medial episodic network. *Trends Cogn Sci*. 2020;24(6):451-465.

47. Das SR, Xie L, Wisse LE, et al.; Alzheimer's Disease Neuroimaging Initiative. Longitudinal and cross-sectional structural magnetic resonance imaging correlates of AV-1451 uptake. *Neurobiol Aging*. 2018;66:49–58.

48. Das SR, Xie L, Wisse L, et al. In vivo measures of tau burden are associated with atrophy in early Braak stage medial temporal lobe regions in amyloid-negative individuals. *Alzheimers Dem*. 2019;15:1286–1295.

49. de Flores R, , Wisse LEM, Das SR, et al. Contribution of mixed pathology to medial temporal lobe atrophy in Alzheimer's disease. *Alzheimers Dem*. 2020;16(6):843–852.

50. Xie L, Wisse LEM, Das SR, et al.; for the Alzheimer's Disease Neuroimaging Initiative. Longitudinal atrophy in early Braak regions in preclinical Alzheimer's disease. *Hum Brain Mapp*. 2020;41(16):4704–4717.

51. Lindberg O, Mårtensson G, Stomrud E, et al. Atrophy of the posterior subiculum is associated with memory impairment, tau- and amyloid-β pathology in non-demented individuals. *Front Aging Neurosci*. 2017;9:306.

52. Witter MP, Amaral DG. The entorhinal cortex of the monkey: VI. Organization of projections from the hippocampus, subiculum, presubiculum and parasubiculum. *J Comp Neurol*. 2021;529(4):828–852.

53. Ferguson MA, Lim C, Cooke D, et al. . A human memory circuit derived from brain lesions causing amnesia. *Nat Commun*. 2019;10(1):3497.

54. Harrison TM, Maass A, Adams JN, Du R, Baker SL, Jagust WJ. Tau deposition is associated with functional isolation of the hippocampus in aging. *Nat Commun*. 2019;10(1):4900.

55. Kaboodvand N, Bäckman L, Nyberg L, Salami A. The retrosplenial cortex: a memory gateway between the cortical default mode network and the medial temporal lobe. *Hum Brain Mapp*. 2018;39(5):2020–2034.

56. Vogel JW, Young AL, Oxtoby NP, et al. Characterizing the spatio-temporal variability of Alzheimer's disease pathology. *medRxiv*. [Preprint] doi:10.1101/2020.08.20.20176883